49. PLOTS OF CROSS SECTIONS AND RELATED QUANTITIES

(For neutrino plots, see review article "Neutrino Cross Section Measurements" by G.P. Zeller in this edition of RPP)

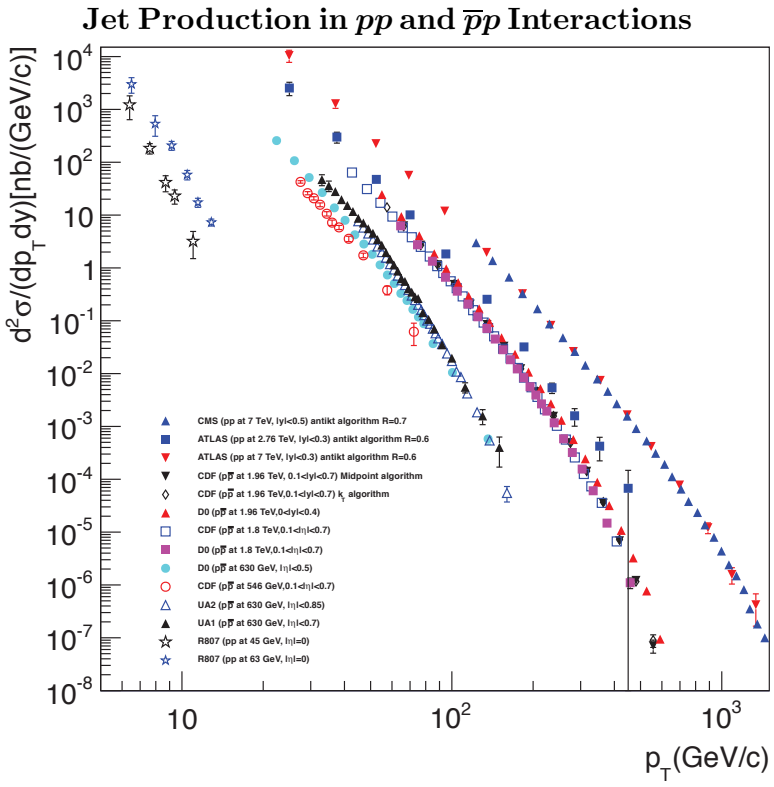

Figure 49.1: Inclusive differential jet cross sections, in the central rapidity region, plotted as a function of the jet transverse momentum. Results earlier than from the Tevatron Run 2 used transverse energy rather than transverse momentum and pseudo-rapidity η rather than rapidity y, but p_T and y are used for all results shown here for simplicity. The error bars plotted are in most cases the experimental stat. and syst. errors added in quadrature. The CDF and D0 measurements use jet sizes of 0.7 (JetClu for CDF Run 1, and Midpoint and k_T for CDF Run 2, a cone algorithm for D0 in Run 1 and the Midpoint algorithm in Run 2). The ATLAS results are plotted for the antikT algorithm for R=0.4, while the CMS results also use antikT, but with R=0.5. NLO QCD predictions in general provide a good description of the Tevatron and LHC data; the Tevatron jet data in fact are crucial components of global PDF fits, and the LHC data are starting to be used as well. Comparisons with the older cross sections are more difficult due to the nature of the jet algorithms used. **ATLAS**:Phys. Rev. **D86**, 014022 (2012), Eur. Phys. J **C73**, 2509 (2013); **CMS**: Phys. Rev. **D84**, 052011 (2011); **CDF**: Phys. Rev. **D75**, 092006 (2007), Phys. Rev. **D64**, 032001 (2001), Phys. Rev. Lett. **70**, 1376 (1993); **D0**: Phys. Rev. **D64**, 032003 (2001); **UA2**: Phys. Lett. **B257**, 232 (1991); **UA1**: Phys. Lett. **172**, 461 (1986); **R807**: Phys. Lett. **B123**, 133 (1983). (Courtesy of J. Huston, Michigan State University, 2013.)

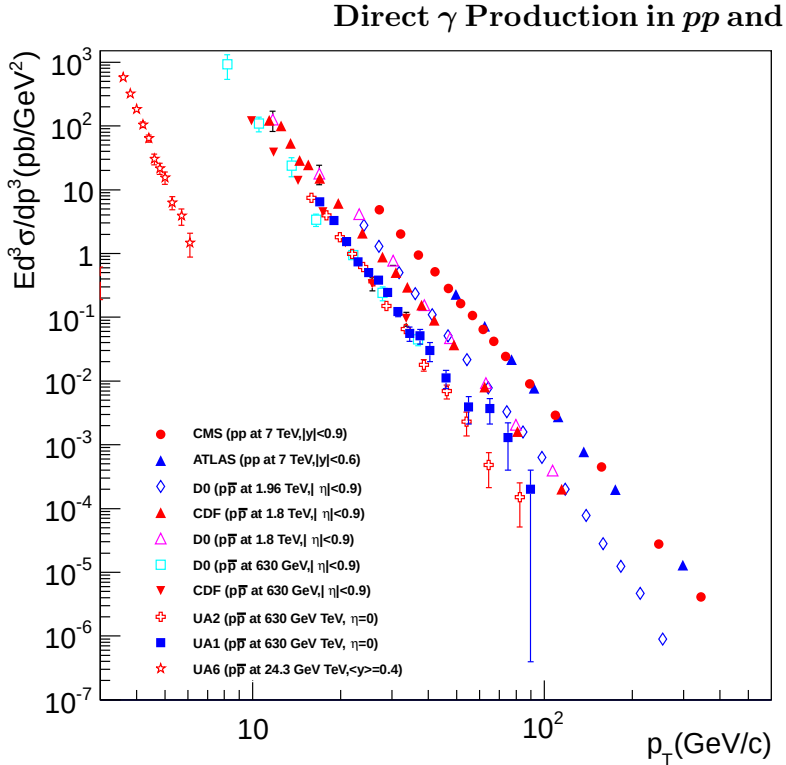

Figure 49.2: Isolated photon cross sections plotted as a function of the photon transverse momentum. The errors are either statistical only, or statistical and systematic added in quadrature. **ATLAS**: Phys. Lett. **B706**, 150 (2011); **CMS**: Phys. Rev. **D84**, 052011 (2011); **D0** : Phys. Lett. **B639**, 151 (2006), Phys. Rev. Lett. **87**, 251805 (2001); **CDF**: Phys. Rev. **D65**, 112003 (2002); **UA6**: Phys. Lett. **B206**, 163 (1988); **UA1**: Phys. Lett. **B209**, 385 (1988); **UA2**: Phys. Lett. **B288**, 386 (1992). (Courtesy of J. Huston, Michigan State University, 2013).

Differential Cross Section for W and Z Boson Production

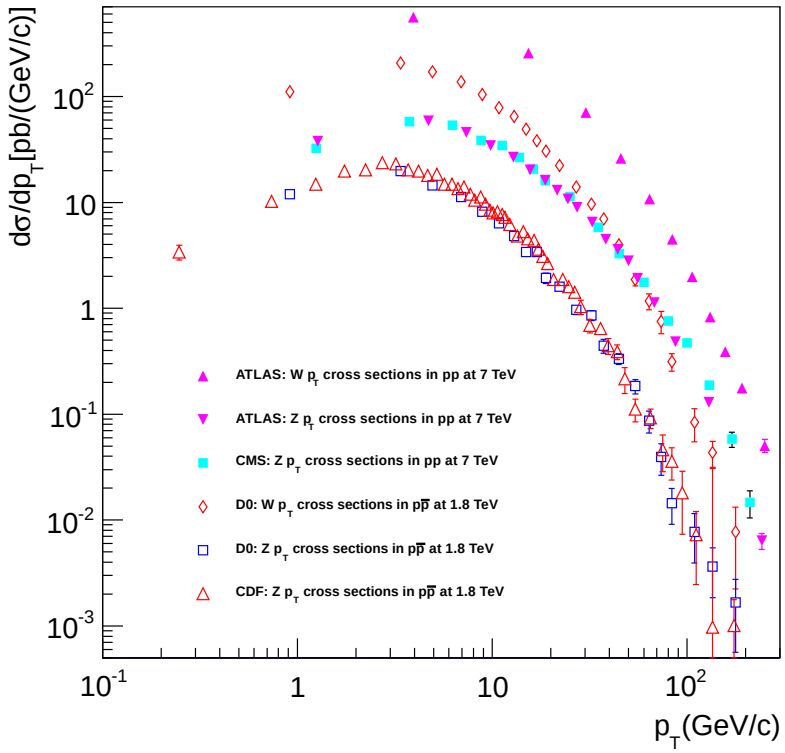

Figure 49.3: Differential cross sections for W and Z production shown as a function of the boson transverse momentum. The errors plotted are either statistical only or statistical and systematic added in quadrature. The results are in good agreement with theoretical predictions that include both the effects of NLO corrections and of q_T resummation. **ATLAS**: Phys. Rev. **D85**, 012005 (2012), Phys. Lett. **B705**, 415 (2011); **CMS**: Phys. Rev. **D85**, 032002 (2012); **D0**: Phys. Lett. **B513**, 292 (2001), Phys. Rev. Lett. **84**, 2792 (2000); **CDF**: Phys. Rev. Lett. **84**, 845 (2000). (Courtesy of J. Huston, Michigan State University, 2013.)

Pseudorapidity Distributions in pp and $\overline{p}p$ Interactions

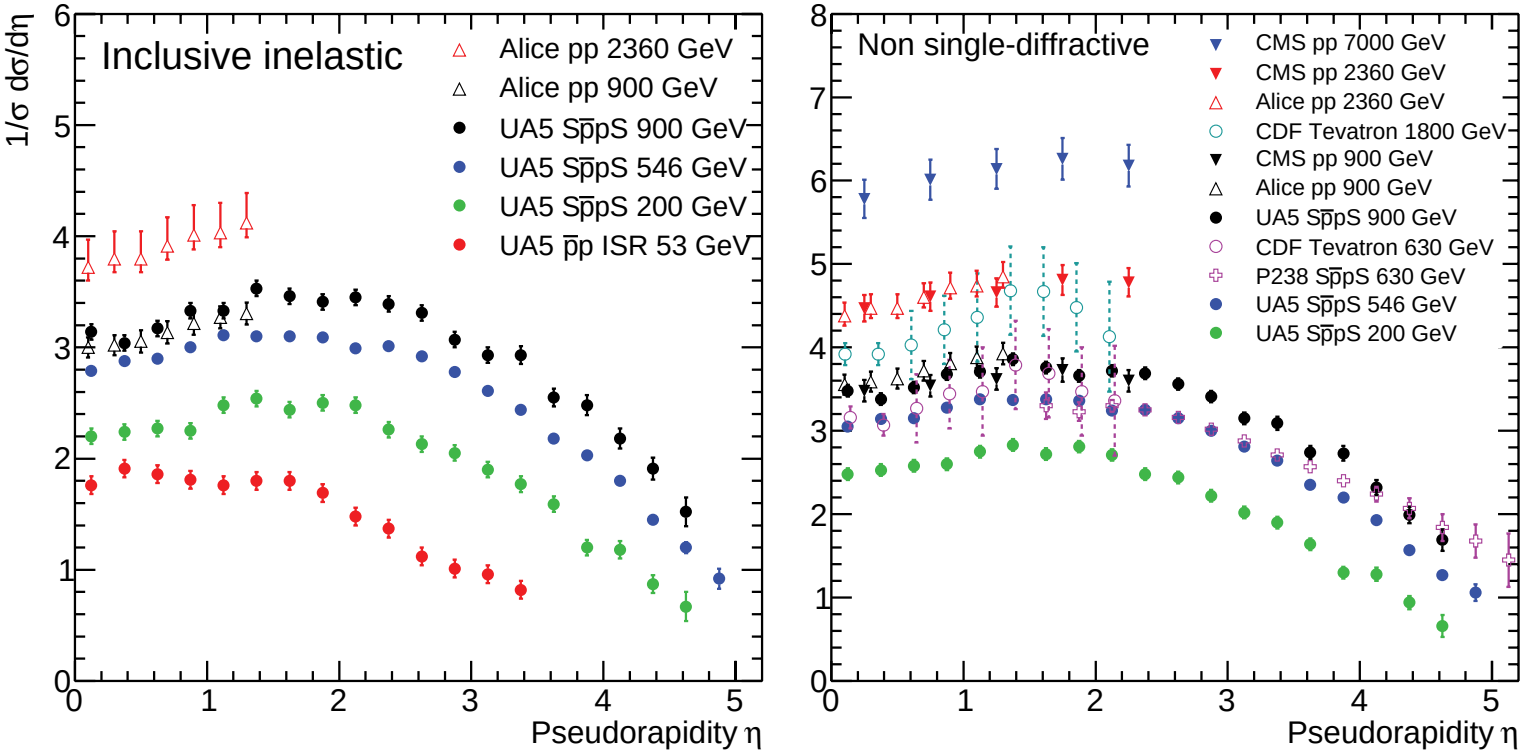

Figure 49.4: Charged particle pseudorapidity distributions in $p\overline{p}$ collisions for 53 GeV $\leq \sqrt{s} \leq$ 1800 GeV. UA5 data from the S$p\overline{p}$S are taken from G.J.Alner *et al.*, Z. Phys. **C33**, 1 (1986), and from the ISR from K.Alpgøard *et al.*, Phys.Lett. 112B 193 (1982). The UA5 data are shown for both the full inelastic cross-section and with singly diffractive events excluded. Additional non single-diffractive measurements are available from CDF at the Tevatron, F.Abe *et al.*, Phys. Rev. **D41**, 2330 (1990) and from P238 at the S$p\overline{p}$S, R.Harr *et al.*, Phys. Lett. **B401**, 176 (1997). These may be compared with both inclusive and non single-diffractive measurements in pp collisions at the LHC from ALICE, K.Aamodt *et al.*, Eur. Phys. J. **C68**, 89 (2010) and for non single-diffractive interactions from CMS , V.Khachatryan *et al.*, JHEP 1002:041 (2010), Phys. Rev. Lett. **105**, 022002 (2010). (Courtesy of D.R. Ward, Cambridge Univ., 2013)

Average Hadron Multiplicities in Hadronic e^+e^- Annihilation Events

Table 49.1: Average hadron multiplicities per hadronic e^+e^- annihilation event at $\sqrt{s} \approx 10$, 29–35, 91, and 130–200 GeV. The rates given include decay products from resonances with $c\tau < 10$ cm, and include the corresponding anti-particle state. Correlations of the systematic uncertainties were considered for the calculation of the averages. (Updated August 2013 by O. Biebel, LMU, Munich)

Particle	$\sqrt{s} \approx 10$ GeV	$\sqrt{s} = 29$–35 GeV	$\sqrt{s} = 91$ GeV	$\sqrt{s} = 130$–200 GeV
Pseudoscalar mesons:				
π^+	6.52 ± 0.11	10.3 ± 0.4	17.02 ± 0.19	21.24 ± 0.39
π^0	3.2 ± 0.3	5.83 ± 0.28	9.42 ± 0.32	
K^+	0.953 ± 0.018	1.48 ± 0.09	2.228 ± 0.059	2.82 ± 0.19
K^0	0.91 ± 0.05	1.48 ± 0.07	2.049 ± 0.026	2.10 ± 0.12
η	0.20 ± 0.04	0.61 ± 0.07	1.049 ± 0.080	
$\eta'(958)$	0.03 ± 0.01	0.26 ± 0.10	0.152 ± 0.020	
D^+	$0.194 \pm 0.019^{(a)}$	0.17 ± 0.03	0.175 ± 0.016	
D^0	$0.446 \pm 0.032^{(a)}$	0.45 ± 0.07	0.454 ± 0.030	
D_s^+	$0.063 \pm 0.014^{(a)}$	$0.45 \pm 0.20^{(b)}$	0.131 ± 0.021	
$B^{(c)}$	—	—	$0.165 \pm 0.026^{(d)}$	
B^+	—	—	$0.178 \pm 0.006^{(d)}$	
B_s^0	—	—	$0.057 \pm 0.013^{(d)}$	
Scalar mesons:				
$f_0(980)$	0.024 ± 0.006	$0.05 \pm 0.02^{(e)}$	0.146 ± 0.012	
$a_0(980)^\pm$	—	—	$0.27 \pm 0.11^{(f)}$	
Vector mesons:				
$\rho(770)^0$	0.35 ± 0.04	0.81 ± 0.08	1.231 ± 0.098	
$\rho(770)^\pm$	—	—	$2.40 \pm 0.43^{(f)}$	
$\omega(782)$	0.30 ± 0.08	—	1.016 ± 0.065	
$K^*(892)^+$	0.27 ± 0.03	0.64 ± 0.05	0.715 ± 0.059	
$K^*(892)^0$	0.29 ± 0.03	0.56 ± 0.06	0.738 ± 0.024	
$\phi(1020)$	0.044 ± 0.003	0.085 ± 0.011	0.0963 ± 0.0032	
$D^*(2010)^+$	$0.177 \pm 0.022^{(a)}$	0.43 ± 0.07	$0.1937 \pm 0.0057^{(g)}$	
$D^*(2007)^0$	$0.168 \pm 0.019^{(a)}$	0.27 ± 0.11	—	
$D_s^*(2112)^+$	$0.048 \pm 0.014^{(a)}$	—	$0.101 \pm 0.048^{(h)}$	
$B^{*\ (i)}$	—	—	0.288 ± 0.026	
$J/\psi(1S)$	$0.00050 \pm 0.00005^{(a)}$	—	$0.0052 \pm 0.0004^{(j)}$	
$\psi(2S)$	—	—	$0.0023 \pm 0.0004^{(j)}$	
$\Upsilon(1S)$	—	—	$0.00014 \pm 0.00007^{(j)}$	
Pseudovector mesons:				
$f_1(1285)$	—	—	0.165 ± 0.051	
$f_1(1420)$	—	—	0.056 ± 0.012	
$\chi_{c1}(3510)$	—	—	$0.0041 \pm 0.0011^{(j)}$	
Tensor mesons:				
$f_2(1270)$	0.09 ± 0.02	0.14 ± 0.04	0.166 ± 0.020	
$f_2'(1525)$	—	—	0.012 ± 0.006	
$K_2^*(1430)^+$	—	0.09 ± 0.03	—	
$K_2^*(1430)^0$	—	0.12 ± 0.06	0.084 ± 0.022	
$B^{**\ (k)}$	—	—	0.118 ± 0.024	
$D_{s1}^\pm$	—	—	$0.0052 \pm 0.0011^{(\ell)}$	
$D_{s2}^{*\pm}$	—	—	$0.0083 \pm 0.0031^{(\ell)}$	
Baryons:				
p	0.266 ± 0.008	0.640 ± 0.050	1.050 ± 0.032	1.41 ± 0.18
Λ	0.080 ± 0.007	0.205 ± 0.010	0.3915 ± 0.0065	0.39 ± 0.03
Σ^0	0.023 ± 0.008	—	0.076 ± 0.011	
Σ^-	—	—	0.081 ± 0.010	
Σ^+	—	—	0.107 ± 0.011	
$\Sigma^\pm$	—	—	0.174 ± 0.009	
Ξ^-	0.0059 ± 0.0007	0.0176 ± 0.0027	0.0258 ± 0.0010	
$\Delta(1232)^{++}$	0.040 ± 0.010	—	0.085 ± 0.014	
$\Sigma(1385)^-$	0.006 ± 0.002	0.017 ± 0.004	0.0240 ± 0.0017	
$\Sigma(1385)^+$	0.005 ± 0.001	0.017 ± 0.004	0.0239 ± 0.0015	
$\Sigma(1385)^\pm$	0.0106 ± 0.0020	0.033 ± 0.008	0.0462 ± 0.0028	
$\Xi(1530)^0$	0.0015 ± 0.0006	—	0.0068 ± 0.0006	
Ω^-	0.0007 ± 0.0004	0.014 ± 0.007	0.0016 ± 0.0003	
Λ_c^+	$0.074 \pm 0.031^{(m)}$	0.110 ± 0.050	0.078 ± 0.017	
Λ_b^0	—	—	0.031 ± 0.016	
$\Sigma_c^{++}, \Sigma_c^0$	0.014 ± 0.007	—	—	
$\Lambda(1520)$	0.008 ± 0.002	—	0.0222 ± 0.0027	

Notes for Table 49.1:

(*a*) $\sigma_{\rm had} = 3.33 \pm 0.05 \pm 0.21$ nb (**CLEO**: Phys. Rev. **D29**, 1254 (1984)) has been used in converting the measured cross sections to average hadron multiplicities.

(*b*) B($D_s \to \eta\pi,\ \eta'\pi$) was used (RPP 1994).

(*c*) Comprises both charged and neutral B meson states.

(*d*) The Standard Model B($Z \to b\overline{b}$) = 0.217 was used.

(*e*) $x_p = p/p_{\rm beam} > 0.1$ only.

(*f*) Both charge states.

(*g*) B($D^*(2010)^+ \to D^0\pi^+$) × B($D^0 \to K^-\pi^+$) has been used (RPP 2000).

(*h*) B($D_s^* \to D_S^+\gamma$), B($D_s^+ \to \phi\pi^+$), B($\phi \to K^+K^-$) have been used (RPP 1998).

(*i*) Any charge state (*i.e.*, B_d^*, B_u^*, or B_s^*).

(*j*) B($Z \to$ hadrons) = 0.699 was used (RPP 1994).

(*k*) Any charge state (*i.e.*, B_d^{**}, B_u^{**}, or B_s^{**}).

(*ℓ*) Assumes B($D_{s1}^+ \to D^{*+}K^0 + D^{*0}K+$) = 100% and B($D_{s2}^+ \to D^0K^+$) = 45%.

(*m*) The value was derived from the cross section of $\Lambda_c^+ \to p\pi K$ using (*a*) and assuming the branching fraction to be (5.0 ± 1.3)% (RPP 2004).

References for Table 49.1:

RPP 1992: Phys. Rev. **D45** (1992); **RPP 1994**: Phys. Rev. **D50**, 1173 (1994); **RPP 1996**: Phys. Rev. **D54**, 1 (1996); **RPP 1998**: Eur. Phys. J. **C3**, 1 (1998); **RPP 2000**: Eur. Phys. J. **C15**, 1 (2000); **RPP 2002**: Phys. Rev. **D66**, 010001 (2002); **RPP 2004**: Phys. Lett. **B592**, 1 (2004); **RPP 2006**: J. Phys. **G33**, 1 (2006); **RPP 2008**: Phys. Lett. **B667**, 1 (2008); **RPP 2010**: J. Phys. **G37**, 075021 (2010); **RPP 2012**: Phys. Rev. D 86,010001(2012) and references therein.

R. Marshall, Rept. on Prog. in Phys. **52**, 1329 (1989). A. De Angelis, J. Phys. **G19**, 1233 (1993) and references therein.

ALEPH: D. Buskulic *et al.*: Phys. Lett. **B295**, 396 (1992); Z. Phys. **C64**, 361 (1994); **C69**, 15 (1996); **C69**, 379 (1996); **C73**, 409 (1997); and R. Barate *et al.*: Z. Phys. **C74**, 451 (1997); Phys. Reports **294**, 1 (1998); Eur. Phys. J. **C5**, 205 (1998); **C16**, 597 (2000); **C16**, 613 (2000); and A. Heister *et al.*: Phys. Lett. **B526**, 34 (2002); **B528**, 19 (2002).

ARGUS: H. Albrecht *et al.*: Phys. Lett. **230B**, 169 (1989); Z. Phys. **C44**, 547 (1989); **C46**, 15 (1990); **C54**, 1 (1992); **C58**, 199 (1993); **C61**, 1 (1994); Phys. Rep. **276**, 223 (1996).

BaBar: B. Aubert *et al.*: Phys. Rev. Lett. **87**, 162002 (2001); Phys. Rev. **D65**, 091104 (2002); J.P. Lees *et al.*: SLAC-PUB-15524, `arXiv:1306.2895`.

Belle: K. Abe *et al.*, Phys. Rev. Lett. **88**, 052001 (2002); and R. Seuster *et al.*, Phys. Rev. **D73**, 032002 (2006).

CELLO: H.J. Behrend *et al.*: Z. Phys. **C46**, 397 (1990); **C47**, 1 (1990).

CLEO: D. Bortoletto *et al.*, Phys. Rev. **D37**, 1719 (1988); erratum *ibid.* **D39**, 1471 (1989); and M. Artuso *et al.*, Phys. Rev. **D70**, 112001 (2004).

Crystal Ball: Ch. Bieler *et al.*, Z. Phys. **C49**, 225 (1991).

DELPHI: P. Abreu *et al.*: Z. Phys. **C57**, 181 (1993); **C59**, 533 (1993); **C61**, 407 (1994); **C65**, 587 (1995); **C67**, 543 (1995); **C68**, 353 (1995); **C73**, 61 (1996); Nucl. Phys. **B444**, 3 (1995); Phys. Lett. **B341**, 109 (1994); **B345**, 598 (1995); **B361**, 207 (1995); **B372**, 172 (1996); **B379**, 309 (1996); **B416**, 233 (1998); **B449**, 364 (1999); **B475**, 429 (2000); Eur. Phys. J. **C6**, 19 (1999); **C5**, 585 (1998); **C18**, 203 (2000); and J. Abdallah *et al.*, Phys. Lett. **B569**, 129 (2003); Phys. Lett. **B576**, 29 (2003); Eur. Phys. J. **C44**, 299 (2005); and W. Adam *et al.*: Z. Phys. **C69**, 561 (1996); **C70**, 371 (1996).

HRS: S. Abachi *et al.*, Phys. Rev. Lett. **57**, 1990 (1986); and M. Derrick *et al.*, Phys. Rev. **D35**, 2639 (1987).

L3: M. Acciarri *et al.*: Phys. Lett. **B328**, 223 (1994); **B345**, 589 (1995); **B371**, 126 (1996); **B371**, 137 (1996); **B393**, 465 (1997); **B404**, 390 (1997); **B407**, 351 (1997); **B407**, 389 (1997), erratum *ibid.* **B427**, 409 (1998); **B453**, 94 (1999); **B479**, 79 (2000).

MARK II: H. Schellman *et al.*, Phys. Rev. **D31**, 3013 (1985); and G. Wormser *et al.*, Phys. Rev. Lett. **61**, 1057 (1988).

JADE: W. Bartel *et al.*, Z. Phys. **C20**, 187 (1983); and D.D. Pietzl *et al.*, Z. Phys. **C46**, 1 (1990).

OPAL: R. Akers *et al.*: Z. Phys. **C63**, 181 (1994); **C66**, 555 (1995); **C67**, 389 (1995); **C68**, 1 (1995); and G. Alexander *et al.*: Phys. Lett. **B358**, 162 (1995); Z. Phys. **C70**, 197 (1996); **C72**, 1 (1996); **C72**, 191 (1996); **C73**, 569 (1997); **C73**, 587 (1997); Phys. Lett. **B370**, 185 (1996); and
K. Ackerstaff *et al.*: Z. Phys. **C75**, 192 (1997); Phys. Lett. **B412**, 210 (1997); Eur. Phys. J. **C1**, 439 (1998); **C4**, 19 (1998); **C5**, 1 (1998); **C5**, 411 (1998); and G. Abbiendi *et al.*: Eur. Phys. J. **C16**, 185 (2000); **C17**, 373 (2000).

PLUTO: Ch. Berger *et al.*, Phys. Lett. **104B**, 79 (1981).

SLD: K. Abe, Phys. Rev. **D59**, 052001 (1999); Phys. Rev. **D69**, 072003 (2004).

TASSO: H. Aihara *et al.*, Z. Phys. **C27**, 27 (1985).

TPC: H. Aihara *et al.*, Phys. Rev. Lett. **53**, 2378 (1984).

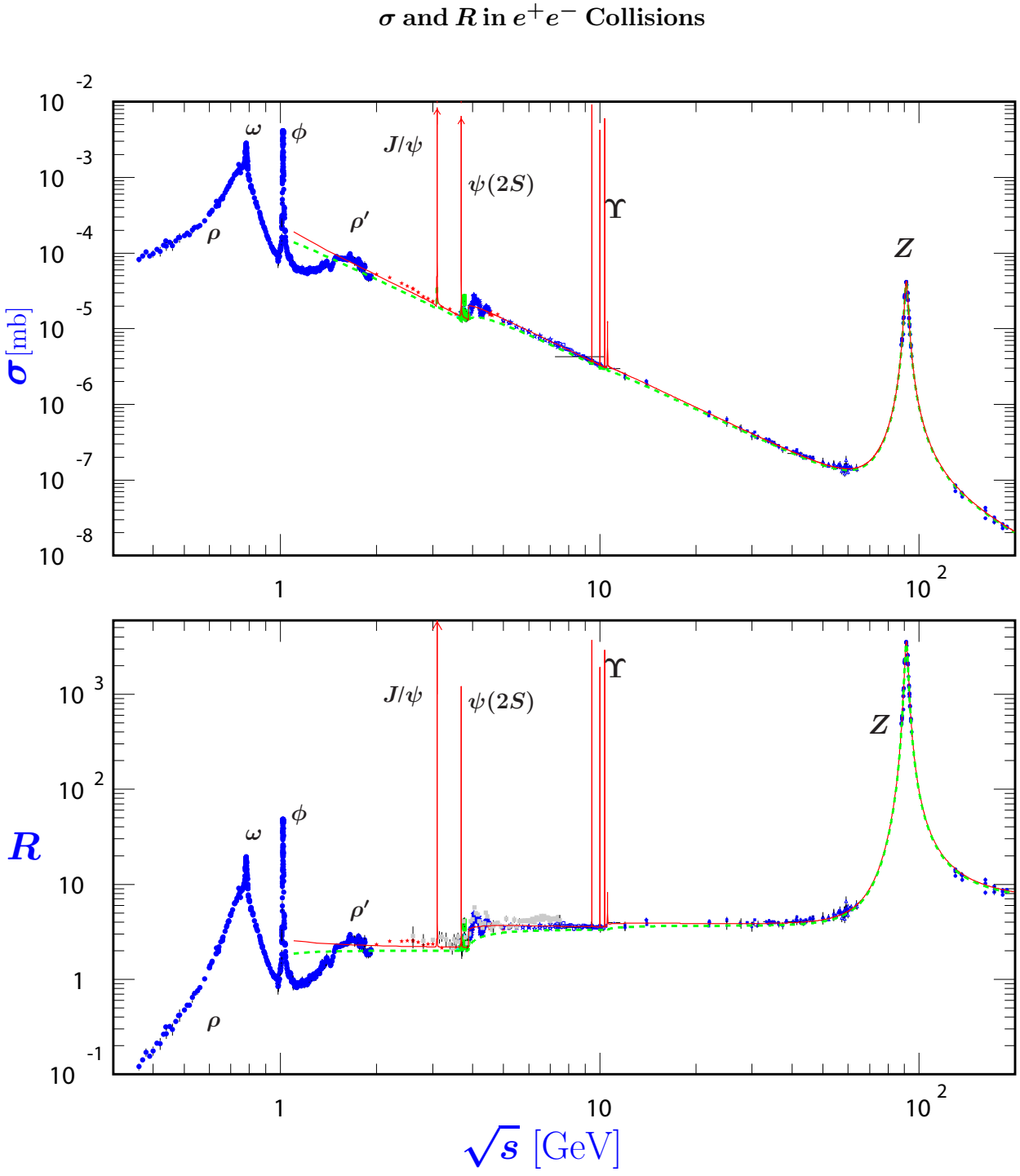

Figure 49.5: World data on the total cross section of $e^+e^- \to hadrons$ and the ratio $R(s) = \sigma(e^+e^- \to hadrons, s)/\sigma(e^+e^- \to \mu^+\mu^-, s)$. $\sigma(e^+e^- \to hadrons, s)$ is the experimental cross section corrected for initial state radiation and electron-positron vertex loops, $\sigma(e^+e^- \to \mu^+\mu^-, s) = 4\pi\alpha^2(s)/3s$. Data errors are total below 2 GeV and statistical above 2 GeV. The curves are an educative guide: the broken one (green) is a naive quark-parton model prediction, and the solid one (red) is 3-loop pQCD prediction (see "Quantum Chromodynamics" section of this *Review*, Eq. (9.7) or, for more details, K. G. Chetyrkin *et al.*, Nucl. Phys. **B586**, 56 (2000) (Erratum *ibid.* **B634**, 413 (2002)). Breit-Wigner parameterizations of J/ψ, $\psi(2S)$, and $\Upsilon(nS), n = 1, 2, 3, 4$ are also shown. The full list of references to the original data and the details of the R ratio extraction from them can be found in `[arXiv:hep-ph/0312114]`. Corresponding computer-readable data files are available at `http://pdg.lbl.gov/current/xsect/`. (Courtesy of the COMPAS (Protvino) and HEPDATA (Durham) Groups, May 2010.)

R in Light-Flavor, Charm, and Beauty Threshold Regions

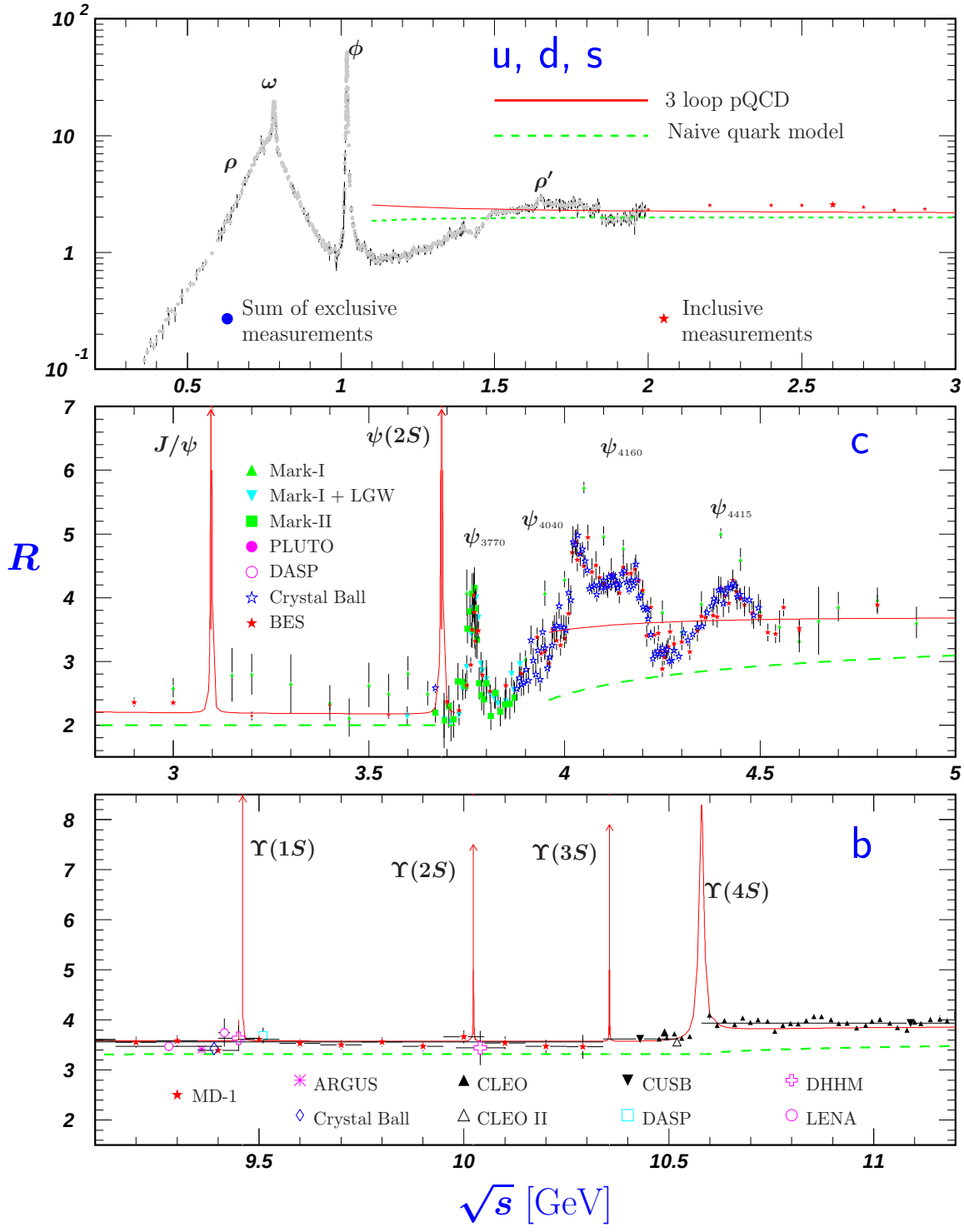

Figure 49.6: R in the light-flavor, charm, and beauty threshold regions. Data errors are total below 2 GeV and statistical above 2 GeV. The curves are the same as in Fig. 49.5. **Note:** CLEO data above $\Upsilon(4S)$ were not fully corrected for radiative effects, and we retain them on the plot only for illustrative purposes with a normalization factor of 0.8. The full list of references to the original data and the details of the R ratio extraction from them can be found in `[arXiv:hep-ph/0312114]`. The computer-readable data are available at `http://pdg.lbl.gov/current/xsect/`. (Courtesy of the COMPAS (Protvino) and HEPDATA (Durham) Groups, May 2010.)

Annihilation Cross Section Near M_Z

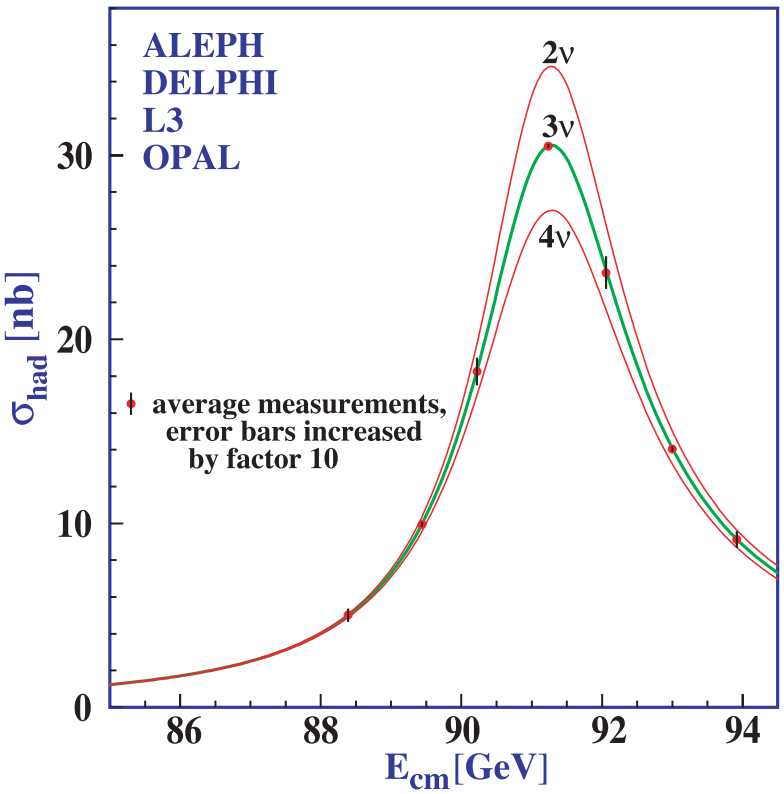

Figure 49.7: Combined data from the ALEPH, DELPHI, L3, and OPAL Collaborations for the cross section in e^+e^- annihilation into hadronic final states as a function of the center-of-mass energy near the Z pole. The curves show the predictions of the Standard Model with two, three, and four species of light neutrinos. The asymmetry of the curve is produced by initial-state radiation. Note that the error bars have been increased by a factor ten for display purposes. References:

ALEPH: R. Barate *et al.*, Eur. Phys. J. **C14**, 1 (2000).
DELPHI: P. Abreu *et al.*, Eur. Phys. J. **C16**, 371 (2000).
L3: M. Acciarri *et al.*, Eur. Phys. J. **C16**, 1 (2000).
OPAL: G. Abbiendi *et al.*, Eur. Phys. J. **C19**, 587 (2001).
Combination: The ALEPH, DELPHI, L3, OPAL, SLD Collaborations, the LEP Electroweak Working Group, and the SLD Electroweak and Heavy Flavor Groups, Phys. Rept. **427**, 257 (2006) [arXiv:hep-ex/0509008].

(Courtesy of M. Grünewald and the LEP Electroweak Working Group, 2007)

Total Hadronic Cross Sections

(Updated September 2013, COMPAS group, IHEP, Protvino)

This updated version of the total hadronic cross sections review is based on the first half of 2013 update of the database for total cross section and the ratio of the real-to-imaginary parts of the forward elastic scattering hadronic amplitudes. New data on total pp collisions cross sections from CERN-LHC-TOTEM [1] and new data from cosmic rays experiment PAO [2] were added.

We use a procedure for ranking models as described in [3] to identify the safest parameterizations for extrapolations. Incidentally, the models giving the best fit of accelerator data also reproduce the experimental cosmic ray nucleon–nucleon data extracted from nucleon–air data with no need of any extra phenomenological corrections to the data.

The statement in [3] that the models with universal (across of collision initial states) $B\log^2(s/s_0)$ asymptotic term work much better than the models with $B\log(s/s_0)$ or $B(s/s_0)^{\Delta}$ terms was confirmed in [4–8] based on matching traditional asymptotic parameterizations with low energy data in different ways. However in these references the scale parameter s_0 was still claimed to be dependent on the colliding particles as it should be for the asymptotic form of parameterizations constructed by the Regge-Gribov phenomenology prescriptions.

The possibility of the universal $\log^2(s/s_0)$ rise of the hadronic total cross sections for different colliding particles was first pointed out by W. Heisenberg [9–10] and discussed many times (see for example [11] and more recent [12–14], and references therein). In [13] the universality of the asymptotic total collision cross sections has been advocated for hadron-nucleus collisions. In [14] additional indications to the universal asymptotic high-energy behavior for hadronic total collision cross sections in form $B\log^2(s/s_0)$ were obtained from lattice QCD.

In this review we use $\mathrm{HPR_1R_2}$ model of highest COMPETE–rank modified (as in 2012 version) to save the universality of the rising part in new form that explicitly includes dependence of the s_0 and B on the initial state mass parameters and the new scale parameter M.

$$\sigma^{a^{\mp}b} = H\log^2\left(\frac{s}{s_M^{ab}}\right) + P^{ab} + R_1^{ab}\left(\frac{s}{s_M^{ab}}\right)^{-\eta_1} \pm R_2^{ab}\left(\frac{s}{s_M^{ab}}\right)^{-\eta_2};$$

$$\rho^{a^{\mp}b} = \frac{1}{\sigma^{a^{\mp}b}}\left[\pi H\log\left(\frac{s}{s_M^{ab}}\right) - R_1^{ab}\left(\frac{s}{s_M^{ab}}\right)^{-\eta_1}\tan\left(\frac{\eta_1\pi}{2}\right) \pm R_2^{ab}\left(\frac{s}{s_M^{ab}}\right)^{-\eta_2}\cot\left(\frac{\eta_2\pi}{2}\right)\right],$$

where upper signs in formulas are for particles and lower signs for antiparticles. The adjustable parameters are as follows:

$H = \pi\frac{(\hbar c)^2}{M^2}$ in mb, where notation $H^{\S}$ is after Heisenberg(1952,1975);

P^{ab} in mb, are Pomeranchuk's(1958) constant terms;

R_i^{ab} in mb are the intensities of the effective secondary Regge pole contributions named after Regge-Gribov(1961);

s, $s_M^{ab} = (m_a + m_b + M)^2$ are in GeV^2 ;

m_a, m_b, $(m_{\gamma^*} = m_{\rho(770)})$ are the masses of initial state particles, and M – the mass parameter defining the rate of universal rise of the cross sections are all in GeV. Parameters M, η_1 and η_2 are universal for all collisions considered.

Exact factorization hypothesis was used for both $H\log^2(\frac{s}{s_M^{ab}})$ and P^{ab} to extend the universal rise of the total hadronic cross sections to the $\gamma(p,d) \to hadrons$ and $\gamma\gamma \to hadrons$ collisions. This results in one additional adjustable parameter δ with substitutions:

$$\pi H\log^2\left(\frac{s}{s_M^{\gamma(p,d)}}\right) + P^{\gamma(p,d)} \Rightarrow \delta\left[\pi(1,\lambda)H\log^2\left(\frac{s}{s_M^{\gamma(p,d)}}\right) + P^{p(p,d)}\right];$$

$$\pi H\log^2\left(\frac{s}{s_M^{\gamma\gamma}}\right) + P^{\gamma\gamma} \quad \Rightarrow \quad \delta^2\left[\pi H\log^2\left(\frac{s}{s_M^{\gamma\gamma}}\right) + P^{pp}\right] \quad .$$

These parameterizations were used for simultaneous fit with **35** adjustable parameters to the data on collisions:

$$(\overline{p},p)\ (p,n,d);\quad \Sigma^- p;\quad \pi^{\mp}\ (p,n,d);\quad K^{\mp}\ (p,n,d);\quad \gamma\ p;\quad \gamma\ \gamma;\quad \gamma\ d.$$

To trace the variation of the range of applicability of simultaneous fit results, several fits were produced with lower energy $\sqrt{s} \geq 5, \geq 6, \geq 7, \ldots$ GeV cutoffs until the uniformity of the fit across different collision became acceptable with good value of FQ.

The results of the fits are presented in the following tables and figures. In the tables, two values of the fit quality indicator $\mathrm{FQ} = \chi^2/(\mathrm{Npt}-35)$ are reported in the last element of the first row for each case of energy cutoff, where **Npt** is the number of data points in corresponding sample. $\mathrm{FQ_{INT}}$ calculated with "internal" parameter values of machine precision (16 digits) and $\mathrm{FQ_{EXT}}$ calculated with rounded parameter values as displayed in the table in accordance with PDG rules (Section 5.3 of J. Beringer *et al.*, (Particle Data Group), Phys. Rev. **D86**, 010001 (2012)), recent metrology recommendations [15] and rules for safe uniform rounding of correlated data [16]. The uniformity of the quality of data description across different collisions is shown in the last two columns of each $\sqrt{s}$ subtable; **npt** is the number of data points in a subsample and χ^2/npt is the contribution of the subsample to the global χ^2 reduced to **npt**. The values of the fit quality indicators and uniformity of model descriptions improve with higher collision energy cuts. The uniformity is excellent for 7 GeV cut. All fits were performed with NonlinearModelFit package in *Mathematica* 8^+, which gives the statistically complete presentation of the fit results: best fit parameter values and estimated parameter uncertainties covariance matrix calculated as inverse $Hessian/2$ matrix at the best fit parameter values which is perfect for linearized in parameters fits, but can produce overestimated covariance matrix for nonlinear optimization task.

---

§ *For collisions with deuteron target H_d=λ H where dimensionless parameter λ is introduced to test the universality of the Heisenberg rise for particle−nuclear and nuclear−nuclear collisions.*

HPR$_1$R$_2$ at $\sqrt{s} \geq 5$GeV	**M**=2.127 ± 0.015 **[GeV]** **H**=0.2704 ± 0.0038 **[mb]** $\eta_1 = 0.451 \pm 0.013$ $\eta_2 = 0.5490 \pm 0.0070$ $\delta = (\mathbf{3.060 \pm 0.021}) \times \mathbf{10^{-3}}$ $\lambda = 1.626 \pm 0.049$			**FQ$_{\mathbf{INT}}$ = 0.96** **FQ$_{\mathbf{EXT}}$ = 0.96**
P[mb]	R_1**[mb]**	R_2**[mb]**	**Beam/Target**	**Npt=1046**	χ^2/npt **by Groups**
34.49 ± 0.21	12.98 ± 0.26	7.38 ± 0.11	$\bar{p}(p)/p$	*256*	*1.15*
34.79 ± 0.25	12.44 ± 0.48	6.65 ± 0.22	$\bar{p}(p)/n$	*67*	*0.48*
34.7 ± 2.0	$-48. \pm 30.$	$-50. \pm 30.$	Σ^-/p	*9*	*0.37*
18.82 ± 0.18	9.48 ± 0.22	1.763 ± 0.042	$\pi^{\mp}/p$	*183*	*1.02*
16.41 ± 0.13	4.22 ± 0.19	3.403 ± 0.060	$K^{\mp}/p$	*121*	*0.81*
16.35 ± 0.14	3.64 ± 0.27	1.82 ± 0.10	$K^{\mp}/n$	*64*	*0.58*
	0.0137 ± 0.0017		γ/p	*41*	*0.62*
	$(-4. \pm 25.) \times 10^{-6}$		γ/γ	*37*	*0.75*
	0.0367 ± 00028		γ/d	*13*	*0.9*
64.59 ± 0.53	29.51 ± 0.61	14.93 ± 0.24	$\bar{p}(p)/d$	*85*	*1.51*
36.75 ± 0.41	18.64 ± 0.58	0.34 ± 0.12	$\pi^{\mp}/d$	*92*	*0.72*
32.13 ± 0.32	7.61 ± 0.48	5.61 ± 0.12	$K\mp/d$	*78*	*0.79*

HPR$_1$R$_2$ at $\sqrt{s} \geq 6$GeV	**M**=2.081 ± 0.016 **[GeV]** **H**=0.2824 ± 0.0044 **[mb]** $\eta_1 = 0.409 \pm 0.016$ $\eta_2 = 0.5566 \pm 0.0083$ $\delta = (\mathbf{3.097 \pm 0.026}) \times \mathbf{10^{-3}}$ $\lambda = 1.496 \pm 0.053$			**FQ$_{\mathbf{INT}}$ = 0.9** **FQ$_{\mathbf{EXT}}$ = 0.9**
P[mb]	R_1**[mb]**	R_2**[mb]**	**Beam/Target**	**Npt=933**	χ^2/npt **by Groups**
34.70 ± 0.31	13.72 ± 0.32	7.58 ± 0.14	$\bar{p}(p)/p$	*243*	*1.13*
34.03 ± 0.34	13.16 ± 0.54	6.88 ± 0.25	$\bar{p}(p)/n$	*58*	*0.45*
34.5 ± 2.1	$-29. \pm 20.$	$-32. \pm 20.$	Σ^-/p	*9*	*0.38*
18.15 ± 0.26	10.20 ± 0.29	1.855 ± 0.055	$\pi^{\mp}/p$	*157*	*0.99*
15.90 ± 0.19	4.93 ± 0.25	3.466 ± 0.077	$K^{\mp}/p$	*99*	*0.7*
15.86 ± 0.20	4.38 ± 0.34	1.83 ± 0.12	$K^{\mp}/n$	*55*	*0.58*
	0.0146 ± 0.0021		γ/p	*35*	*0.59*
	$(-18. \pm 27.) \times 10^{-6}$		γ/γ	*34*	*0.75*
	0.0315 ± 00035		γ/d	*6*	*1.06*
64.48 ± 0.68	27.53 ± 0.78	15.36 ± 0.33	$\bar{p}(p)/d$	*77*	*1.06*
36.43 ± 0.56	18.19 ± 0.72	0.38 ± 0.13	$\pi^{\mp}/d$	*87*	*0.7*
32.97 ± 0.32	7.36 ± 0.60	5.71 ± 0.14	$K\mp/d$	*73*	*0.72*

HPR$_1$R$_2$ at $\sqrt{s} \geq 7$GeV	**M**=2.076 ± 0.016 **[GeV]** **H**=0.2838 ± 0.0045 **[mb]** $\eta_1 = 0.412 \pm 0.017$ $\eta_2 = 0.5626 \pm 0.0092$ $\delta = (\mathbf{3.112 \pm 0.027}) \times \mathbf{10^{-3}}$ $\lambda = 1.456 \pm 0.058$			**FQ$_{\mathbf{INT}}$ = 0.86** **FQ$_{\mathbf{EXT}}$ = 0.87**
P[mb]	R_1**[mb]**	R_2**[mb]**	**Beam/Target**	**Npt=933**	χ^2/npt **by Groups**
33.73 ± 0.33	13.67 ± 0.33	7.77 ± 0.18	$\bar{p}(p)/p$	*219*	*1.09*
33.77 ± 0.38	14.05 ± 0.63	6.93 ± 0.29	$\bar{p}(p)/n$	*48*	*0.39*
33.2 ± 3.9	$-14. \pm 47.$	$-15. \pm 52.$	Σ^-/p	*8*	*0.41*
18.08 ± 0.29	10.44 ± 0.32	1.977 ± 0.078	$\pi^{\mp}/p$	*137*	*0.91*
15.84 ± 0.20	5.12 ± 0.28	3.538 ± 0.095	$K^{\mp}/p$	*85*	*0.76*
15.73 ± 0.22	4.81 ± 0.40	1.86 ± 0.13	$K^{\mp}/n$	*48*	*0.56*
	0.0132 ± 0.0023		γ/p	*34*	*0.56*
	$(-60. \pm 33.) \times 10^{-6}$		γ/γ	*31*	*0.68*
	0.0256 ± 00044		γ/d	*3*	*0.31*
64.79 ± 0.75	27.06 ± 0.85	15.46 ± 0.37	$\bar{p}(p)/d$	*75*	*0.97*
36.66 ± 0.62	17.89 ± 0.82	0.38 ± 0.14	$\pi^{\mp}/d$	*81*	*0.71*
32.28 ± 0.46	7.02 ± 0.71	5.74 ± 0.16	$K\mp/d$	*67*	*0.67*

Cut in GeV	Λ_5^{min}	CN_5	Λ_6^{min}	CN_6	Λ_7^{min}	CN_7
Hessian	*0.000093*	*137197*	*0.000190*	*69375*	*0.000034*	*353613*
Monte Carlo	*0.00047*	*27022*	*0.00090*	*14345*	*0.00086*	*14452*
$\mid MC_{cut} \mid$	*1000000*		*200000*		*300000*	

To construct the parameter scatter region we follow Section 37.4.2.2 of J. Beringer *et al.*. (Particle Data Group), Phys. Rev. **D86**, 010001 (2012) and recent metrology JCGM 101:2008 recommendations and produce the direct Monte Carlo propagation of uncertainties from experimental data to the uncertainties of the best fit parameters. To do this we interpret the whole input data sample as statistically independent sample with total experimental uncertainty at each experimental data point being a Gaussian standard deviation. This technical assumption allows us to generate MC sampling of experimental data and to obtain at each MC trial new "biased" best fit parameters belonging to scatter region of the initial best fit parameters values. These biased best fit parameters constitute the MC-samples of cardinalities $|MC_{cut}|$ at each $\sqrt{s}$ cutoff and are the basis for construction of three 35-dimensional empirical parameter distributions. These distributions were used to estimate correlation matrices and compare their characteristics: minimal eigenvalues Λ_{cut}^{min} and condition numbers defined as $CN_{cut} = \Lambda_{cut}^{max}/\Lambda_{cut}^{min}$ with that of estimates obtained by Hessian method (see the bottom subtable). The results show that the MC-matrices are better than the Hessian matrices in all the cases. Condition numbers are much smaller.

It should be stressed that almost all best fit parameters are monotonously shifted as the lower $\sqrt{s}$ cutoff increases. The shifts are within 2 to 3 standard deviations and in "expected" directions. Indeed:

• λ is expected from [13] to weakly depend on atomic numbers of colliding nuclei and asymptotically tend to 1 as $\sqrt{s} \to \infty$, its $\sqrt{s}$ dependence being quite weak;

• Rate H of Heisenberg rise is increasing;

• Scale M (defining the starting point $s = s_M^{ab}$ of Heisenberg's rise) is decreasing towards the possible mass of lightest glueball or alternatively towards the $s_M^{ab} = m_a \cdot m_b$. Regge-Gribov prescriptions to construct asymptotic hadronic scattering amplitudes is based on transition to complex valued $z_t \gg 1$ (z_t– the cosine of t-channel scattering angle expressed in s-channel Mandelstam variables). Condition $z_t \gg 1$ for s-channel forward scattering amplitudes is equivalent to $\frac{s}{m_a \cdot m_b} \gg 1$. Thus, the energy scale in all nonlinear entries of z_t in asymptotic expressions is fixed. This "expected" monotonic evolution of asymptotic parameters with growth of $\sqrt{s}$ cutoff indicates that hadronic "asymptopia" clearly starts above the 7 GeV border. The rise of H with $\sqrt{s}$ cut could be treated as indication to the possible changes in the functional energy dependence of the leading asymptotic term to the $log^c(s/s_0)$ with $c > 2$ or even to temporal power behavior $(s/s_0)^{\Delta}$. In a recent paper [17] the asymptotic bounds (Froissart, Martin) on the possible rise of the total collision cross sections in the form $log^2(s/s_0)$ was questioned in favour of possible faster rising forms. It was supported by the fits presented in [18] where the form $\log^c(s/s_0)$ with adjustable c was tested on $(\bar{p})pp$ data only and it was claimed that values of c obtained in number of different fits are statistically compatible with $c \in [2.2, 2.4]$.

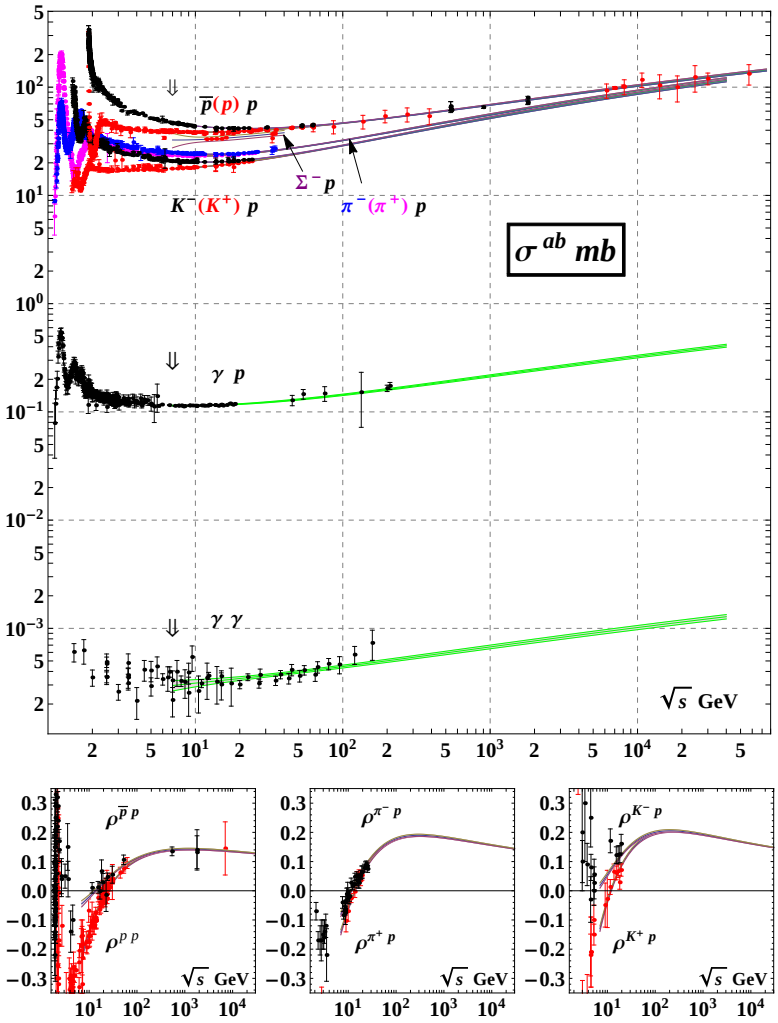

Figure 49.8: Summary of $h^{\mp}p \to anything$, $\gamma p \to hadrons$, $\gamma\gamma \to hadrons$ total cross sections σ^{ab} in mb and $\rho^{h^{\mp}p}$ the ratio of real to imaginary parts of the forward hadronic amplitudes. Also for qualitative comparison of the uniformity of data description by HPR_1R_2–model across the different collisions and observables. The uncertainties for the experimental data points include both the statistical and systematic errors. Curves, corresponding to fit above 7 GeV cut, are plotted with error bands calculated with parameter covariance matrix constructed on MC-propagated vectors from 95% quantile of the empirical distribution.

We have performed our global fit with adjustable c to the total cross sections and available ρ–parameters (as of August 2013) including TOTEM data point at 8 TeV [18]. For this fit we have 37 adjustable parameters. Fit was done with all data at $\sqrt{s} \geq 5$ GeV with $FQ = 0.87$. We have obtained value $c = 1.98 \pm 0.01$ (Hessian error) which is in two standard deviation lower than $c = 2$(exact) and possibly could be tentatively interpreted as an indication to the slower universal rising total cross sections as it was proposed 33 years ago by Cheng and Wu in the form $\log^2\left(\frac{(s/s_0)^a}{\log^2(s/s_0)}\right)$ in their seminal paper [20]. However, to notice this difference much experimental, theoretical, and modelling work has to be done. In conclusion, the Heisenberg prediction of the universal $\log^2(s/s_M)$ form of asymptotic rise of the hadronic collision total cross sections is still actual and should be tested in all aspects at available colliders operating with $(\bar{p}, p, nuclei)$ beams and in experiments with cosmic rays.

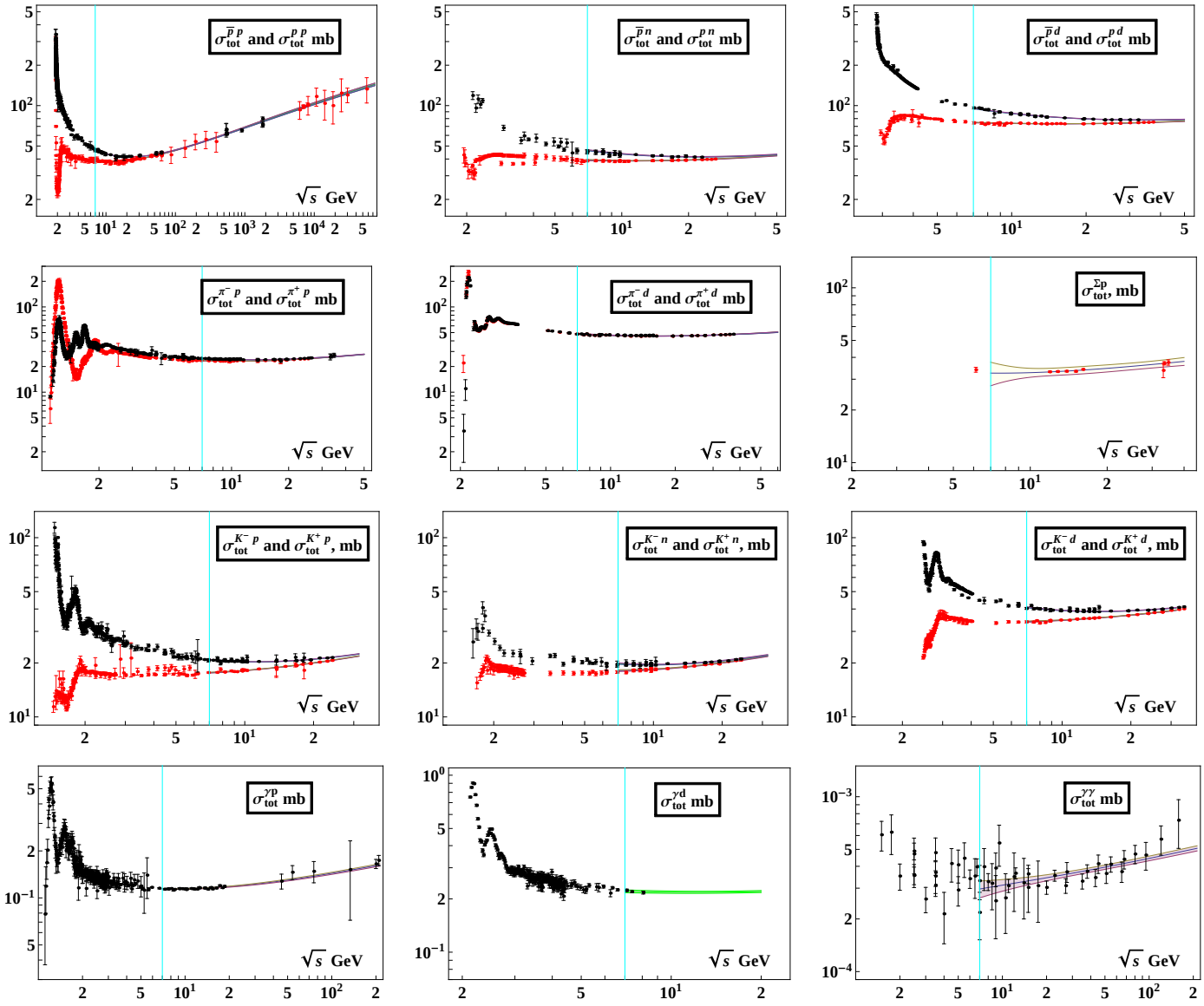

Figure 49.9: Summary of all total collision cross sections jointly fitted with available hadronic ρ parameter data. Corresponding computer-readable data files may be found at http://pdg.lbl.gov/xsect/contents.html

References

[1] G. Antchev *et al.*, Europhys. Lett. **101**, 21004 (2013).

[2] P. Abreu *et al.*, Phys. Rev. Lett. **109**, 062002 (2012).

[3] J.R. Cudell *et al.*: Phys. Rev. **D65**, 074024 (2002); Phys. Rev. Lett. **89**, 201801 (2002).

[4] K. Igi and M. Ishida: Phys. Rev. **D66**, 034023 (2002); Phys. Lett. **B622**, 286 (2005).

[5] M.M. Bock and F. Halzen: Phys. Rev. **D72**, 036006 (2005); Phys. Rev. **D72**, 039902 (2005).

[6] M. Ishida and K. Igi, Prog. Theor. Phys. Suppl. **187**, 297 (2011).

[7] M. Ishida and V. Barger, Phys. Rev. **D84**, 014027 (2011).

[8] F. Halzen *et al.*, Phys. Rev. **D85**, 074020 (2012).

[9] W. Heisenberg, Z. Phys. **133**, 65 (1952).

[10] W. Heisenberg, *Fourteenth Int. Cosm. Ray Conference*, Vol.11, München 1975, 3461-3474;

[11] S.S. Gershtein and A.A. Logunov, Sov. J. Nucl. Phys. **39**, 960 (1984).

[12] E. Iancu and R. Venugopalan, R.C. Hwa (ed.) *et al.*, [hep-ph/0303204].

[13] L. Frankfurt, M. Strikman, and M. Zhalov, Phys. Lett. **B616**, 59 (2005).

[14] M. Giordana, E. Meggiolaro, and N. Moretti, JHEP **1209**, 031 (2012).

[15] JCGM 100:2008, JCGM 101:2008, JCGM 104:2009, JCGM 102:2011 via www.bipm.org/en/publications/guides/gum.html

[16] V.V. Ezhela, Data Science Journal **6**, PS676 (2007).

[17] Y.I. Azimov, Phys. Rev. **D84**, 056012 (2011).

[18] D.A. Fagundes, M.J. Menon, and P.V.R.G. Silva, J. Phys. **G40**, 065005 (2013).

[19] G. Antchev *et al.*, Phys. Rev. Lett. **111**, 012001 (2013).

[20] H. Cheng and T.T. Wu, Phys. Rev. Lett. **24**, 145 (1970).

High Energy Elastic $\bar{p}\,p$ and $p\,p$ Differential Cross Sections

(Updated September 2013, COMPAS group, IHEP, Protvino)

Using new results from FNAL-COLLIDER-D0 experiment in $\bar{p}\,p$ elastic collisions at $\sqrt{s} = 1.96$ TeV [1], CERN-LHC-TOTEM experiment in $p\,p$ elastic collisions at $\sqrt{s} = 7$, 8 TeV [2–3] and PAO experiment in proton-air collisions at 57 TeV [4] the amplitudes of the elastic $\bar{p}\,p$ and $p\,p$ collisions are investigated in a most broad region in $\sqrt{s}$ and t via three observables $d\sigma/dt(s,t)$, $\sigma^{tot}(s)$, and $\rho(s)$. The summary of the database for $d\sigma/dt(s,t)$ is presented in Figure 49.10, where projection of the $d\sigma/dt(\sqrt{s},t)$ to the $(d\sigma/dt, -t)$ plane orthogonal to the $\sqrt{s}$ axis is displayed.

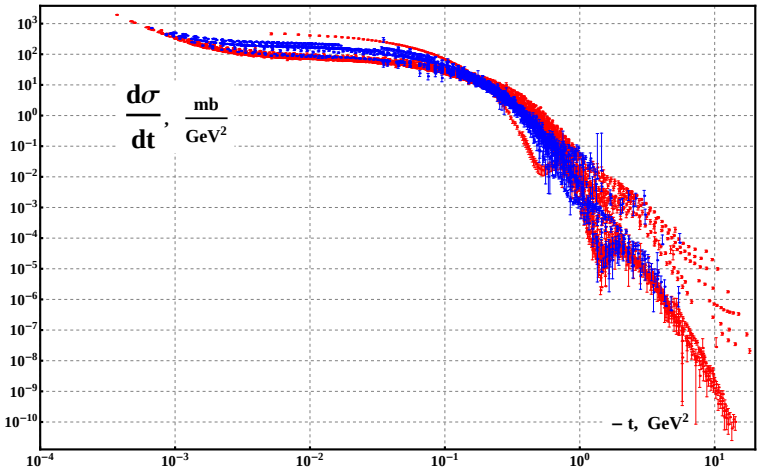

Figure 49.10: Cumulative plots of data on $d\sigma/dt$ for $\bar{p}\,p$ (blue) and $p\,p$ (red) elastic collisions at $\sqrt{s} \geq 2.99$ GeV. Number of data points $Ntot = 6629$

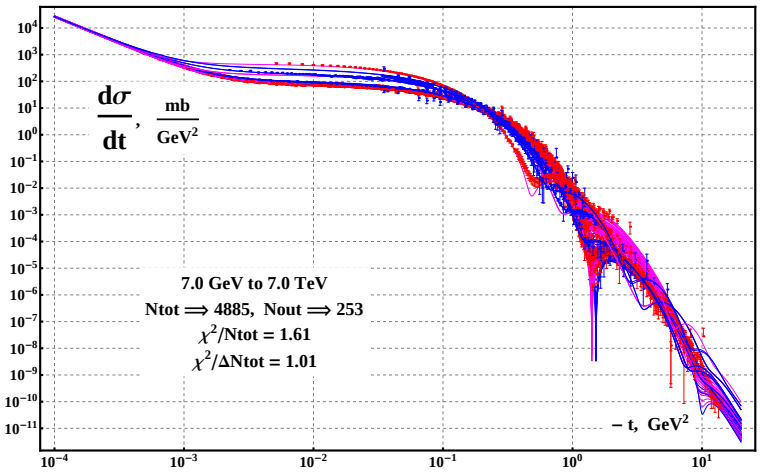

Figure 49.11: Cumulative plots of data on $d\sigma/dt$ and model description for $\bar{p}\,p$ (blue,blue) and $p\,p$ (red,magenta) elastic collisions at $\sqrt{s} \geq 7$ GeV.

All characteristic features of the $d\sigma/dt(\sqrt{s},t)$ behavior in $-t$ and $\sqrt{s}$ are clearly seen:

- The energy-dependent Coulomb-Nuclear Interference (CNI) effects at small $-t$;
- Diffractive peaks with crossover effect at $-t \approx 0.16\,\mathrm{GeV}^2$ for particle-antiparticle data at same energies;
- The first dip/shoulder moving to the left with growing $\sqrt{s}$. New data on $d\sigma/dt$ in $\bar{p}\,p$ and $p\,p$ elastic collisions at highest accelerator energies have challenged all previous model predictions that gave "not so bad qualitative agreement" with previously available data on $d\sigma/dt$. There is a need to reveal a quantitative and statistically complete picture of the data description by at least one model with most ambitious claim on the "best known description". There are several conceptually related papers with such a claims [5–7] but with different areas of applicability and without treatment of the CNI region. Description of $d\sigma/dt$ by our model (a variation of AGNM [7] parameterization) at $\sqrt{s} \geq 7$ GeV is displyed on Figure 49.11. Our model which includes terms responsible for the CNI effects gives stable fit quality (FQ) for the whole sample with all available values of $-t$. Overall $FQ = 1.51$ and reduced to $d\sigma/dt$ $FQ(d\sigma/dt) \approx 1.61$.

Historically the most complete compilations on $d\sigma/dt$ data expressed in Mandelstam variables $\sqrt{s}$ and t were published in Landolt-Börnstein volumes (now available in digital form) up to 1981 [8]. Updated (in high energy part) analogous CLM-compilation [9] (available in computer readable form) was compiled with help of HEPDATA and COMPAS databases and released in 2006. In our fits we use the CLM-compilation with minor corrections, filled detected gaps, and updated with new data published up to August 2013. We performed simultaneous fits to the sample of data on $d\sigma/dt(s,t)$, $\sigma^{tot}(s)$, and $\rho(s)$ in $\bar{p}\,p$ and $p\,p$ collisions at $7\,\mathrm{GeV} \leq \sqrt{s} \leq 8\,\mathrm{TeV}$ and all available t. Overall fit quality $FQ = \chi^2(Ntot)/(Ntot - Npar) = 1.51$, which is unreliable for our number of degrees of freedom. Removing contributions to $\chi^2(d\sigma/dt)$ from $Nout = 253$ points with $\chi^2(point) > (2.4)^2$ (of 2.4×standard deviation (**std**) – randomly scattered outliers) we have $\chi^2(\Delta Ntot)/(\Delta Ntot) = 1.01$, where $\Delta Ntot = Ntot - Nout$. The uniformity level of the fit quality in different intervals of $\sqrt{s}$ is shown on Figure 49.12.

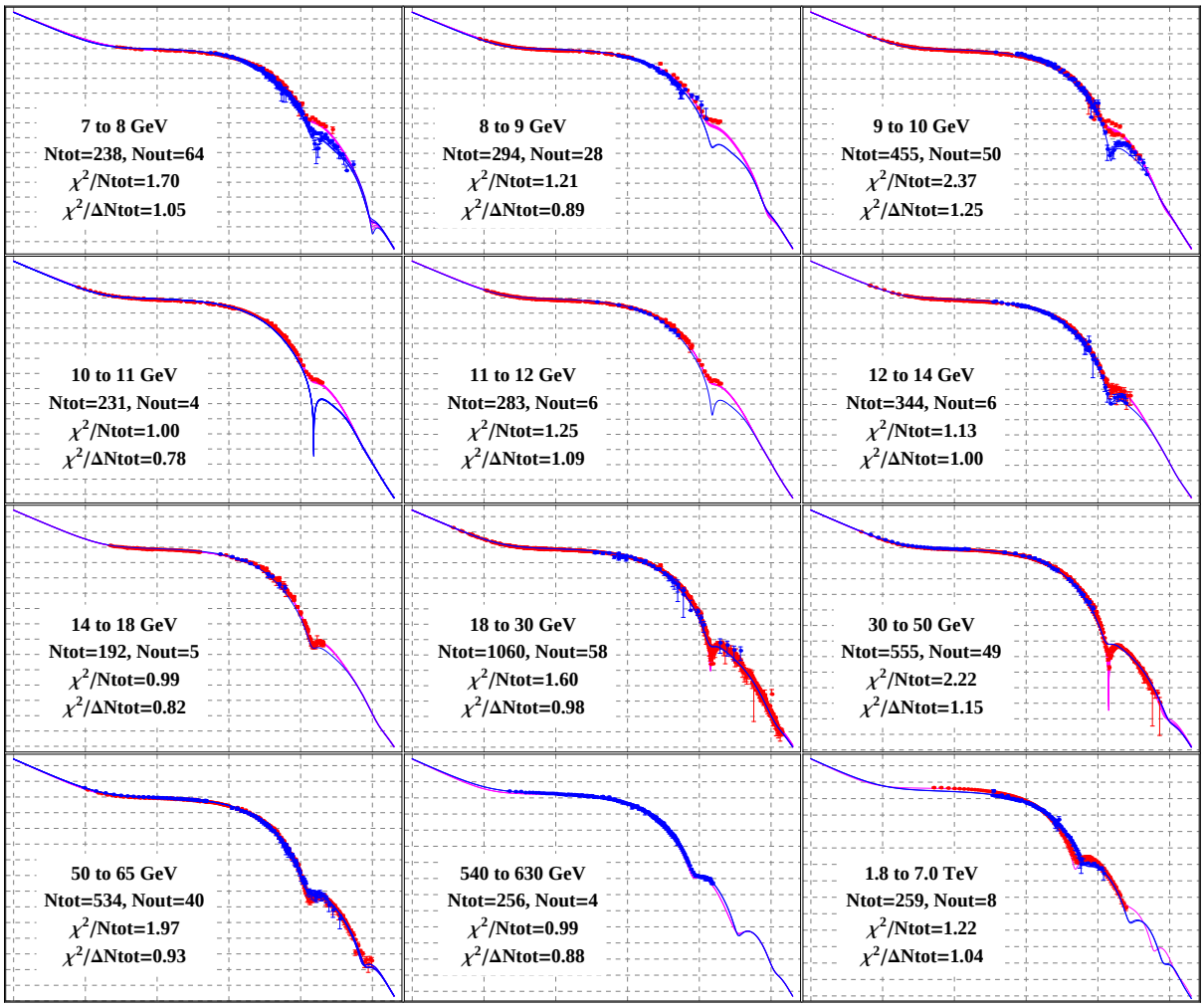

Figure 49.12: All 12 energy intervals are non overlapping and cover all data points. All panels have axis labelled as in Figure 49.11. All data sets corresponding to the same energy have model curve drawn. Some panels have no red or blue data points. In such a cases we add the curve as prediction of the model.

To reveal a more complete picture of phenomenological description of the elastic scattering data we originally selected the most flexible model (43 parameters) from [7] with most broad claimed area of applicability. It turns out that without partial removal of some data (made in [7]) the claimed solution cannot be used even as starting point for adjustments, most probably, because of over-rounded published parameter values, or misprints in parameter tables, or strong parameter correlations. Moreover, numerous fits with different starting points failed to find any locally stable solution with physically reasonable adjustable parameter values. We obtain a stable solution only with addition of data in CNI region and with slightly modified parameterization to reduce the number of adjustable parameters from 43 to 37. Our expressions for observables $\sigma_{\pm}^{tot}(s)$, $\rho_{\pm}(s)$, and $d\sigma_{\pm}/dt(s,t)$ with sign "+" for pp and sign "−" for $\bar{p}p$ collisions are constructed (in notations of [7]) using corresponding scattering amplitudes: nuclear $T_{\pm}(s,t)$ and Coulomb $T_{\pm}^{c}(s,t)$ both in mb $\cdot$ GeV^2 as follows:

$$\sigma_{\pm}^{tot}(s) = \frac{Im\ \ T_{\pm}(s,0)}{\sqrt{s(s-4m_p^2)}}, \qquad \rho_{\pm}(s) = \frac{Re\ \ T_{\pm}(s,0)}{Im\ \ T_{\pm}(s,0)}, \qquad \frac{d\sigma_{\pm}}{dt}(s,t) = \frac{\left|T_{\pm}(s,t)+T_{\pm}^{c}(s,t)\right|^2}{16\pi(\hbar c)^2 s(s-4m_p^2)},$$

where constants: m_p stands for proton mass, and $(\hbar c)^2$ for mb-to-GeV^2 conversion factor. Nuclear amplitudes $T_{\pm}(s,t)$ are linearly combined crossing even $F_{+}(\hat{s},t)$ and crossing odd $F_{-}(\hat{s},t)$ functions.

$$T_{\pm}(s,t) = [F_{+}(\hat{s},t) \mp F_{-}(\hat{s},t)],$$

$$F_{+}(\hat{s},t) = F_{+}^{H}(\hat{s},t) + F_{+}^{P}(\hat{s},t) + F_{+}^{PP}(\hat{s},t) + F_{+}^{R}(\hat{s},t) + F_{+}^{RP}(\hat{s},t) + N_{+}(s,t),$$

$$F_{-}(\hat{s},t) = F_{-}^{MO}(\hat{s},t) + F_{-}^{O}(\hat{s},t) + F_{-}^{OP}(\hat{s},t) + F_{-}^{R}(\hat{s},t) + F_{-}^{RP}(\hat{s},t) + N_{-}(s,t),$$

$$F_{+}^{H}(\hat{s},t) = i\hat{s}\left\{\begin{array}{c} H_1\dfrac{2J_1(K_+\tilde{\tau})}{K_+\tilde{\tau}}\cdot e^{b_{+1}t}\ln^2\tilde{s}\ + \\ H_2 J_0(K_+\tilde{\tau})\cdot e^{b_{+2}t}\ln\tilde{s}\quad + \\ H_3\left[J_0(K_+\tilde{\tau}) - K_+\tilde{\tau}J_1(K_+\tilde{\tau})\right]\cdot e^{b_{+3}t} \end{array}\right\}, \qquad F_{-}^{MO}(\hat{s},t) = \hat{s}\left\{\begin{array}{c} O_1\dfrac{\sin(K_-\tilde{\tau})}{K_-\tilde{\tau}}e^{b_{-1}t}\cdot\ln^2\tilde{s}\ + \\ O_2\cos(K_-\tilde{\tau})e^{b_{-2}t}\cdot\ln\tilde{s}\quad + \\ O_3\ \ e^{b_{-3}t} \end{array}\right\},$$

$$F_+^P(\hat{s},t) = -C_P e^{b_P t} e^{-i\frac{\pi}{2}\alpha_P(t)}\,(\hat{s})^{\alpha_P(t)}\,, \qquad F_-^O(\hat{s},t) = -iC_O e^{b_O t} e^{-i\frac{\pi}{2}\alpha_O(t)}\,(\hat{s})^{\alpha_O(t)}\,(1+A_O t),$$

$$F_+^{PP}(\hat{s},t) = -\frac{C_{PP}}{\ln\tilde{s}} e^{b_{PP} t} e^{-i\frac{\pi}{2}\alpha_{PP}(t)}\,(\hat{s})^{\alpha_{PP}(t)}\,, \quad F_-^{OP}(\hat{s},t) = -i\frac{C_{OP}}{\ln\tilde{s}} e^{b_{OP} t} e^{-i\frac{\pi}{2}\alpha_{OP}(t)}\,(\hat{s})^{\alpha_{OP}(t)}\,,$$

$$F_\pm^{RP}(\hat{s},t) = \frac{tC_{RP}^\pm}{\ln\tilde{s}} e^{b_{RP}^\pm t} i\frac{-1\pm1}{2}\, e^{-i\frac{\pi}{2}\alpha_{RP}^\pm(t)}\,(\hat{s})^{\alpha_{RP}^\pm(t)}\,, \quad F_\pm^R(\hat{s},t) = \mp C_R^\pm e^{b_R^\pm t} i\frac{-1\pm1}{2}\, e^{-i\frac{\pi}{2}\alpha_R^\pm(t)}\,(\hat{s})^{\alpha_R^\pm(t)}\,,$$

$$N_\pm(s,t) = -i^{\frac{1\pm1}{2}}\cdot\hat{s}\cdot N_\pm\cdot(\ln\tilde{s})\,\frac{t}{t_0}\cdot(1-t/t_\pm)^{-5},$$

$$\alpha_P(t) = 1+\alpha'_P\cdot t; \quad \alpha_R^\pm(t) = \alpha_R^\pm(0)+\alpha_R^{\pm\prime}\cdot t; \quad \alpha_O(t) = 1+\alpha'_O\cdot t\ ,$$

$$\alpha_{OP}(t) = 1+\frac{\alpha'_P\alpha'_O}{\alpha'_P+\alpha'_O}\cdot t; \quad \alpha_{PP}(t) = 1+\frac{\alpha'_P}{2}\cdot t; \quad \alpha_{RP}^\pm(t) = \alpha_R^\pm(0)+\frac{\alpha_P{}'\alpha_R^{\pm\prime}}{\alpha_P{}'+\alpha_R^{\pm\prime}}\cdot t\ ,$$

$$\hat{s}(s,t)\equiv\hat{s} = (-t+2s-4m_p^2)/(2s_0), \ \ s_0 = 1\ \text{GeV}^2; \quad \tilde{s} = \ln\hat{s} - i\frac{\pi}{2}; \quad \tilde{\tau} = \sqrt{-t/t_0}\ln\tilde{s}, \ \ t_0 = 1\ \text{GeV}^2.$$

Coulomb amplitudes are taken with dipole electric nucleon form factor

$$T_\pm^c(s,t) = \mp e^{\left[\pm i\alpha\Phi_\pm^{NC}(s,t)\right]}\cdot 8\pi(\hbar c)^2\alpha\cdot\frac{s}{t}\cdot\left(1-\frac{t}{\Lambda^2}\right)^{-4},$$

where: $\Phi_\pm^{CN}(s,t) = \ln\left[-\frac{t}{2}\left(B_\pm(s)+\frac{8}{\Lambda^2}\right)\right]+\gamma-\frac{4t}{\Lambda^2}\ln\left(-\frac{4t}{\Lambda^2}\right)-\frac{2t}{\Lambda^2}$ is the CNI phase in the R. Cahn form [10]; $\Lambda = \sqrt{0.71}$ GeV; α – fine structure constant; γ – Euler constant. Instead of the traditional definition of the $d\sigma_\pm/dt(s,t)$ slope function $B_\pm(s) = \left[\frac{d}{dt}\ln\left(\frac{d\sigma_\pm}{dt}(s,t)\right)\right]_{t=0}$, we set $B_\pm(s) = \frac{\sigma_\pm(s)}{4\pi(\hbar c)^2}$ to simplify calculations and to get faster minimization procedures. Solution obtained with this simplification is presented in the Table of independently rounded best fit parameter values and their standard deviations.

Name	Unit	Value	±Vstd	Name	Unit	Value	±Vstd
H_1	*mb GeV*^{2}	*0.2478*	*0.0014*	O_1	*mb GeV*^{2}	*0.*	*(fix)*
H_2	*mb GeV*^{2}	*0.0078*	*0.0011*	O_2	*mb GeV*^{2}	*0.686*	*0.049*
H_3	*mb GeV*^{2}	*11.22*	*0.32*	O_3	*mb GeV*^{2}	*-3.82*	*0.51*
K_+		*0.3076*	*0.0017*	K_-		*0.0998*	*0.0029*
C_P	*mb GeV*^{2}	*-0.150*	*0.026*	C_O	*mb GeV*^{2}	*-8.60*	*0.44*
C_{PP}	*mb GeV*^{2}	*148.4*	*2.8*	C_{OP}	*mb GeV*^{2}	*64.1*	*2.3*
C_R^+	*mb GeV*^{2}	*-26.6*	*2.3*	C_R^-	*mb GeV*^{2}	*99.1*	*3.7*
C_{RP}^+	*mb GeV*^{2}	*-1.5*	*1.0*	C_{RP}^-	*mb GeV*^{2}	*-58.0*	*10.0*
$\alpha_R^+(0)$		*0.614*	*0.022*	$\alpha_R^-(0)$		*0.444*	*0.011*
$\alpha_R^{+\prime}$	*GeV*$^{-2}$	*0.8*	*(fix)*	$\alpha_R^{-\prime}$	*GeV*$^{-2}$	*0.8*	*(fix)*
$\alpha_P{}'$	*GeV*$^{-2}$	*0.151*	*0.013*	$\alpha_O{}'$	*GeV*$^{-2}$	*0.947*	*0.099*
b_{+1}	*GeV*$^{-2}$	*3.592*	*0.053*	b_{-1}	*GeV*$^{-2}$	*0.*	*(fix)*
b_{+2}	*GeV*$^{-2}$	*0.622*	*0.021*	b_{-2}	*GeV*$^{-2}$	*3.013*	*0.054*
b_{+3}	*GeV*$^{-2}$	*5.44*	*0.13*	b_{-3}	*GeV*$^{-2}$	*2.572*	*0.069*
b_P	*GeV*$^{-2}$	*0.205*	*0.070*	b_O	*GeV*$^{-2}$	*12.25*	*0.53*
b_{PP}	*GeV*$^{-2}$	*5.643*	*0.071*	b_{OP}	*GeV*$^{-2}$	*2.611*	*0.049*
b_R^+	*GeV*$^{-2}$	*1.92*	*0.13*	b_R^-	*GeV*$^{-2}$	*11.28*	*0.43*
b_{RP}^+	*GeV*$^{-2}$	*0.41*	*0.14*	b_{RP}^-	*GeV*$^{-2}$	*1.27*	*0.14*
N_+	*mb GeV*^{2}	*-0.0441*	*0.0073*	N_-	*mb GeV*^{2}	*9.5*	*2.4*
t_+	*GeV*^{2}	*1.678*	*0.072*	t_-	*GeV*^{2}	*0.190*	*0.014*
				A_O	*GeV*$^{-2}$	*-26.1*	*2.3*

Estimates of the std were obtained by the MC-propagation of the assumed Gaussian distribution for each individual data point. Despite of poor MC statistics, the obtained "propagated" covariance matrix is in good conditions [11] and gives reasonable std estimates. The quality of the fit reduced to the $\sigma_\mp^{tot}(s)$ and $\rho_\mp(s)$ is presented on the Figure 49.13. Error bands were calculated by propagation of the parameter scatter region to the scatter region of these observables.

In summary, the solution obtained gives satisfactory picture of the used parametric description of the current database on observables related to elastic (anti)proton–proton scattering amplitudes, and reveals problems with lack of good data at the pre-asymptotic energies. Indeed:

1. Noisy data in dip/shoulder regions does not allow to tune parameters to give credible description of the depth of dips;

2. All frames in Figure 49.12 with $\sqrt{s}\le 12$ GeV apparently show that there is an urgent need in $\bar{p}p$ data at CNI as well as at the first dip/shoulder "$-t$" intervals;

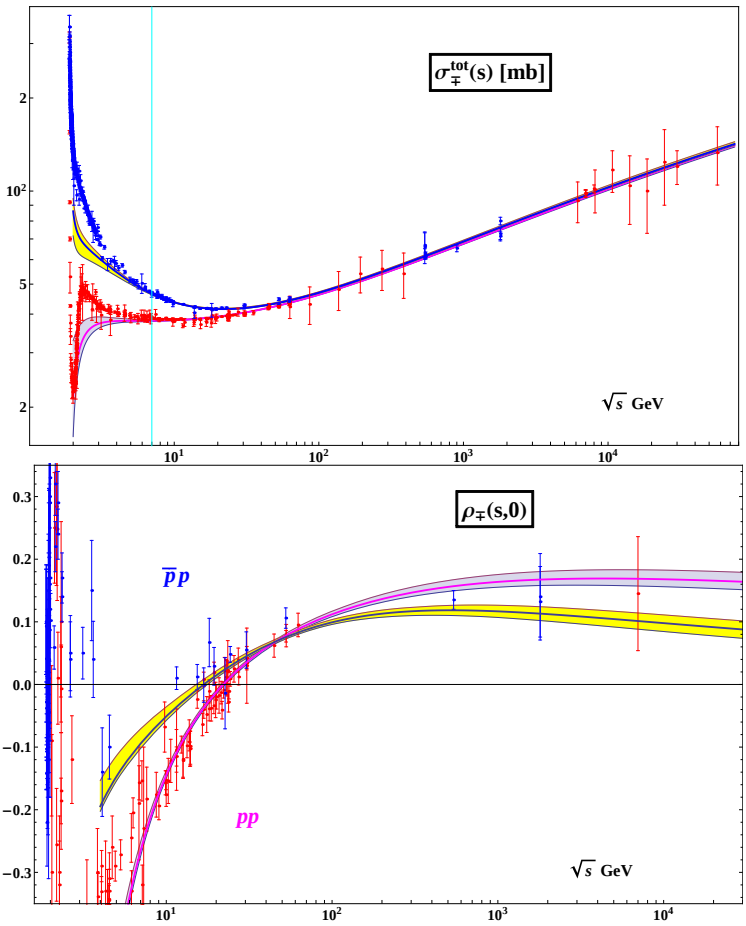

Figure 49.13: Descriptions of $\sigma_{\mp}^{tot}(s)$ and $\rho_{\mp}(s)$ data using our model which is based on AGNM [7] parametrization.

3. Frame marked as "9 to 10 GeV" shows some contradictory data samples in pp collisions (48 "2.4–std outliers" out of 565 data points). There are no model independent resolution of these contradictions other than remeasurements with much higher statistics and more precise measuring systems. New accurate experimental data are highly desirable;

4. There is a sharp difference in descriptions of ρ parameter data from our global fits with HPR_1R_2 model without odderon contribution (non-intersecting $\rho_{\mp}$ curves) and model RPP2013 with odderons (intersecting $\rho_{\mp}$ curves). Further modelling is needed to remove this difference.

In paper [12] the simultaneous description of $\sigma_{\mp}$ and $\rho_{\mp}$ in the interval $5.\text{GeV} \leq \sqrt{s} \leq 7.\text{TeV}$ and $d\sigma_{\mp}/dt$ in the region $(19.\,\text{GeV} \leq \sqrt{s} \leq 7.\,\text{TeV}) \otimes (0.01\,\text{GeV}^2 \leq -t \leq 14.2\,\text{GeV}^2)$ by a hybrid model of [6] and [7] with triple pole odderon switched off at $t = 0$ was claimed to be good enough. It gives nonintersecting $\rho_{\mp}$ curves. Unfortunately the poorly specified pre–filtered experimental data sample to fit, and no evidence of the results stability did not allow us to reproduce claimed results.

Interesting indication on a possible second dip/shoulder "activity" effects at higher values of "$-t$" is visible (on RPP2013 curves) on the first three low energy panels of Figure 49.12 and more pronounced on the last four highest energy panels. The possibility of the multiple dips on the $d\sigma/dt$ at large $|t|$ has been broadly discussed earlier in context of the geometrical picture of diffractive scattering (see, for example, paper [13] and its citations). This could be possibly tested in a dedicated experiments on the high intensity ($\bar{p}$) and p fixed target accelerators and at active colliders. New high precision elastic data at Serpukhov, RHIC, and FNAL energies will be helpful to clarify the situation with multiple dips and odderons in continuing frontier studies by the TOTEM collaboration at CERN-LHC.

References

[1] V.M. Abazov *et al.*, Phys. Rev. **D86**, 012009 (2012);

[2] G. Antchev *et al.*, Europhys. Lett.:**111**, 012001 (2013); **101**, 21004 (2013); **101**, 21002 (2013); **96**, 21002 (2011).

[3] G. Antchev *et al.*, Europhys. Lett. **95**, 41001 (2011).

[4] P. Abreu *et al.*, Phys. Rev. Lett. **109**, 062002 (2012).

[5] R. Avila, Y. Gauron, and B. Nicolescu, Eur. Phys. J. **C56**, 57 (2008).

[6] E. Martynov, Phys. Rev. **D76**, 074030 (2007).

[7] E. Martynov and B. Nicolescu, Eur. Phys. J. **C56**, 57 (2008).

[8] In Landolt-Börnstein, Group I: P.J. Carson, v.9, 675 (1980); R.R. Shubert, v.9, 216 (1980); P.J. Carlson, v.7, 109 (1973); A.N. Diddens, v.7, 27 (1973).

[9] J. R. Cudell, A. Lengyel, and E. Martynov, Phys. Rev. **D73**, 034008 (2006).

[10] R. Cahn, Z. Phys. **C15**, 253 (1982).

[11] Our sample contains 656 37-dimensional vectors in the scatter region. Minimal eigenvalue of the correlation matrix is 8.1×10^{-4}, its condition number is 1.04×10^4.

[12] E. Martynov, Phys. Rev. **D87**, 114018 (2013).

[13] T.T. Chou and C.N. Yang, Phys. Rev. **D19**, 3268 (1979).